ACS APPLIED MATERIALS & INTERFACES

Research Article

www.acsami.org

In Situ ATR and DRIFTS Studies of the Nature of Adsorbed CO_2 on Tetraethylenepentamine Films

Walter Christopher Wilfong,[†] Chakravartula S. Srikanth,[†,‡] and Steven S. C. Chuang*[,§]

[†]Department of Chemical and Biomolecular Engineering and [§]Department of Polymer Science, FirstEnergy Advance Energy Research Center, The University of Akron, Akron, Ohio 44325, United States

Supporting Information

ABSTRACT: CO_2 adsorption/desorption onto/from tetraethylenepentamine (TEPA) films of 4, 10, and 20 μm thicknesses were studied by in situ attenuated total reflectance (ATR) and diffuse reflectance infrared Fourier transform spectroscopy (DRIFTS) techniques under transient conditions. Molar absorption coefficients for adsorbed CO_2 were used to determine the CO_2 capture capacities and amine efficiencies (CO_2/N) of the films in the DRIFTS system. Adsorption of CO_2 onto surface and bulk NH_2 groups of the 4 μm film produced weakly adsorbed CO_2, which can be desorbed at 50 °C by reducing the CO_2 partial pressure. These weakly adsorbed CO_2 exhibit low ammonium ion intensities and could be in the form of ammonium-carbamate ion pairs and zwitterions. Increasing the film thickness enhanced the surface amine−amine interactions, resulting in strongly adsorbed ion pairs and zwitterions associated with NH and NH_2 groups of neighboring amines. These adsorbed species may form an interconnected surface network, which slowed CO_2 gas diffusion into and diminished access of the bulk amine groups (or amine efficiency) of the 20 μm film by a minimum of 65%. Desorption of strongly adsorbed CO_2 comprising the surface network could occur via dissociation of NH_3^+/NH_2^+···NH_2/NH ionic hydrogen bonds beginning from 60 to 80 °C, followed by decomposition of $NHCOO^-$/$NCOO^-$ at 100 °C. These results suggest that faster CO_2 diffusion and adsorption/desorption kinetics could be achieved by thinner layers of liquid or immobilized amines.

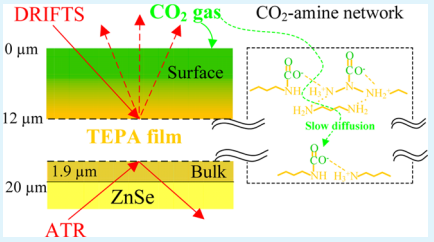

KEYWORDS: *carbon dioxide, amine, film, diffusion, in situ infrared spectroscopy*

INTRODUCTION

A 15% increase in atmospheric CO_2 concentration over the last 20 years[1] to 398 ppm in 2014 and its recognized impact on climate changes have promoted extensive research for the development of effective approaches in controlling CO_2 emissions from the power plants and other point sources. Amine functional groups in the form of (i) aqueous amines: monoethanolamine (MEA)[2−7] and 2-amino-2-methyl-1-propanol (AMP);[8−10] (ii) amine-based ionic liquids (IL's): lysine-based $[N_{66614}][Lys]$[11] and $[EMIM][Lys]$,[12] anionic $[P_{66614}][p\text{-}AA]$,[13] and glycinate-based $[P_{4444}][Gly]$;[14] and (iii) immobilized amines for sorbents and membranes: tetraethylenepentamine (TEPA)[15−19] and polyethylenimine (PEI)[20−25] have been widely studied for capturing the emitted carbon dioxide. Aqueous amines and IL's used for CO_2 absorption have also been incorporated into the sorbents and membranes for CO_2 adsorption.

The reaction mechanisms of CO_2 with aqueous or immobilized primary and secondary amine groups could occur via two general steps,[26−28]

Primary amine:

$$R\text{-}NH_2 + CO_2 \rightarrow R\text{-}NH_2{}^+COO^- \text{ (zwitterion)} \quad (1)$$

$$R\text{-}NH_2{}^+COO^- + {}^*R\text{-}NH_2 \rightarrow R\text{-}NHCOO^- + {}^*R\text{-}NH_3{}^+ \text{ (ion pair)} \quad (2)$$

Secondary amine:

$$R_1\text{-}NH\text{-}R_2 + CO_2 \rightarrow R_1\text{-}NH^+COO^-\text{-}R_2 \text{ (zwitterion)} \quad (1)$$

$$R_1\text{-}NH^+COO^-\text{-}R_2 + {}^*R_1\text{-}NH\text{-}R_2 \rightarrow R_1\text{-}NCOO^-\text{-}R_2 + {}^*R1\text{-}NH_2{}^+\text{-}R_2 \text{ (ion pair)} \quad (2)$$

where $^*R\text{-}NH_2$ represents a second amine molecule. Step 1 proceeds by nucleophilic addition of 1 mol of R-NH_2 (primary) or R_1-NH-R_2 (secondary) amine groups to the carbons of 1 mol of CO_2, forming 1 mol of ammonium-carbamate zwitterion intermediates. The zwitterions are then deprotonated in Step 2 by 1 mol of free amine groups, producing 1 mol of ammonium-carbamate ion pairs. Alternatively, 1 mol of CO_2 could react with 1 mol of primary or secondary amine to form the zwitterion followed by carbamic acid (NHCOOH or NCOOH). It has been reported that carbamic acids are stabilized through the formation of dimers or through hydrogen bonding with neighboring amine groups,[29,30] which has been supported by density functional theory (DFT) calculations.[13] The proposed reactions of CO_2 with the primary amine are further illustrated in Scheme 1.

Received: May 19, 2014
Accepted: July 23, 2014
Published: July 23, 2014

   dx.doi.org/10.1021/am5031006 | ACS Appl. Mater. Interfaces 2014, 6, 13617−13626

Scheme 1. Proposed Reaction Mechanisms of CO_2 with a Primary Amine

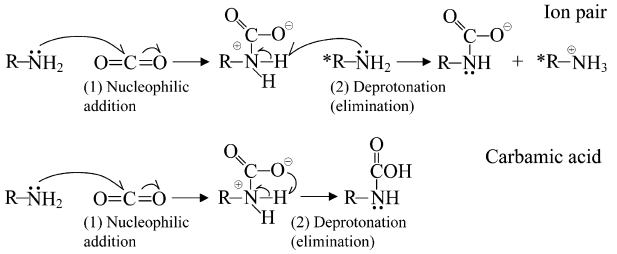

CO_2 diffusion within immobilized polyethylenimine (PEI)/silica sorbents could resemble the facilitated CO_2 diffusion across the amine-containing membranes.[31,32] This type of diffusion has been examined in detail by thermodynamic and kinetic modeling of thermogravimetric analysis (TGA) profiles for adsorbed CO_2 and by performing DFT calculations of different CO_2/amine systems.[33] The mass transfer of CO_2 through the PEI layers was modeled in two steps: (i) the formation of ammonium/carbamate zwitterions (reactive intermediates) and ion pairs at the gas-amine interface followed by (ii) the facilitated diffusion of zwitterions into the bulk. The model revealed that the zwitterion stability (enthalpy and entropy of formation) and its dissociation with an activation energy barrier could control the overall CO_2 uptake kinetics and capacity of the amine sorbent.

Our previous results from a diffuse reflectance infrared Fourier transform spectroscopy (DRIFTS) study showed that CO_2 adsorption onto immobilized TEPA/silica sorbents with a high density of amine sites produced ammonium-carbamate ion pairs and carbamic acid, which inhibited the diffusion of CO_2 gas within the sorbent.[34] Higher density of these ion pairs and acid was envisioned at the external pore mouths of the sorbent rather than inside of the pores of the sorbents with higher amine density at the external particle surface. These results could aid our understanding of the factors in controlling CO_2 gas diffusion into liquid amines. During CO_2 adsorption, a concentration gradient of adsorbed species is formed along the direction of diffusion through liquid and supported amines. A better understanding of the nature of these adsorbed species at different locations within the amine film could provide the scientific basis for the design of more efficient amine sorbents and membranes.

The nature of adsorbed CO_2 at the top surface (7−9 nm) and within the bulk of a 100 μm layer of an NH-containing ionic liquid, dihydroxyethyldimethylammonium taurinate, has been examined by attenuated total reflectance (ATR) and X-ray photoelectron spectroscopy (XPS).[35] The XPS results showed a higher amount of carbamic acid (0.43 mol CO_2/mol IL) than carbamate (0.15 mol CO_2/mol IL) at the top surface than in the bulk of the IL after exposure to 0.9 mbar of CO_2. The ATR and ^{13}C NMR results confirmed the presence of only carbamate species within the bulk after exposure of the IL to 1 bar of CO_2. It was postulated that CO_2 adsorption occurred first at the top surface of the IL by forming carbamic acid followed by carbamates, which then diffused into the bulk. XPS results also showed that CO_2 adsorption onto a 15 μm diameter jet of 30 wt % aqueous MEA solution resulted in neutral MEA molecules at the outer surface layers and carbamate plus carbamic acid species within the bulk layers.[36] It was postulated that CO_2 adsorbed onto the surface of MEA as the carbamate and acid, which diffused (facilitated diffusion) into the bulk.

The objective of this study was to investigate the nature of adsorbed CO_2 on tetraethylenepentamine (TEPA) films. TEPA was selected because it has been widely used for immobilized amine sorbents.[15,19,37−39] We compared the attenuated total reflectance (ATR) and diffuse reflectance (DRIFTS) infrared spectra of adsorbed species during CO_2 adsorption onto and desorption from TEPA films with different thicknesses under transient conditions. Because ATR and DRIFTS should scan the bottom and top layers of the amine films, respectively, the results obtained from these IR studies could provide insights into the mechanisms of the reaction and mass transfer processes occurring near the film surface and within the bulk. We found that adsorption of CO_2 onto TEPA films produced a thick, interconnected network of ammonium-carbamate ion pairs near the film surface, which slowed down CO_2 gas diffusion into and adsorption onto the bulk NH_2 groups. We also estimated the DRIFTS molar absorption coefficients of carbamate and ammonium ions and determined the CO_2/N efficiencies of the films. The latter was found to decrease with increasing thickness, which confirmed the inability of CO_2 to access all available NH and NH_2 groups within the bulk

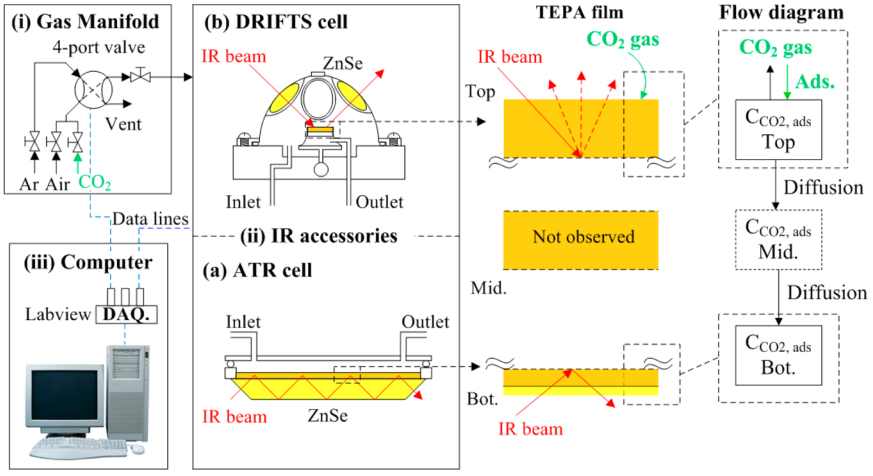

Figure 1. Experimental setup for conducting the CO_2 adsorption−desorption studies.

because of the diffusion limitations imposed by the surface network.

EXPERIMENTAL SECTION

Preparation of Amine Films. Tetraethylenepentamine (TEPA) (Sigma-Aldrich, technical grade) films with nominal thicknesses of 4, 10, and 20 μm were deposited onto (i) the ZnSe crystal of an attenuated total reflectance (ATR) FTIR cell and (ii) a stainless steel metal disk set inside of a diffuse reflectance infrared Fourier transform spectroscopy (DRIFTS) cell for CO_2 adsorption/desorption studies. Different amounts and concentrations of TEPA/ethanol solutions were injected onto the ZnSe crystal and metal disk, which were heated at 80 to 100 °C under a 150 cm^3/min Ar flow to evaporate ethanol. The total amount of TEPA/ethanol solution required to deposit the 4, 10, and 20 μm films are as follows: 200 μL of 0.084, 0.210, and 0.419 M for the 8 cm^2 ATR ZnSe crystal and 5 μL of 0.23, 0.58, and 1.16 M for the 0.55 cm^2 DRIFTS metal disk.

CO_2 Adsorption and Desorption Study. Figure 1 shows the experimental setup used for the CO_2 adsorption and desorption studies, consisting of (i) a gas manifold with mass flow controllers and a 4-port valve for switching the gases between 15% CO_2/air and Ar; (ii-a) an attenuated total reflectance (ATR, Harrick Scientific) accessory with a ZnSe crystal or (ii-b) a stainless steel metal disk set inside of a diffuse reflectance infrared Fourier transform spectroscopy (DRIFTS, Thermo Scientific) cell; and (iii) a Labview DAQ module to operate the 4-port valve and to control and monitor the IR cell temperature. The IR cells and accessories were placed inside of a Fourier transform infrared spectrometer (Nicolet 6700 FTIR, Thermo-Nicolet).

The schematic at the right of Figure 1 illustrates the method for investigating CO_2 adsorption onto and diffusion through the TEPA films by incorporating both IR techniques. Briefly, DRIFTS spectra allowed observation and elucidation of processes of CO_2 gas adsorption near the CO_2/TEPA interface and diffusion into the top of the film. Adsorbed CO_2 continues to diffuse through the middle of the film and reach the bottom of the film, which is shown by the ATR spectra.

In-situ CO_2 adsorption and desorption studies of the TEPA films consists of the following steps: (i) pretreating at 100 °C for 5 min in a 150 cm^3/min Ar flow and cooling to 50 °C, (ii) adsorbing CO_2 for 10 min by step switching to a 150 cm^3/min flow of 15% CO_2/air via the 4-port valve, (iii) removing gas-phase and weakly adsorbed CO_2 by switching back to the Ar flow for 10 min, and (iv) heating to 100 °C at 10 °C/min in Ar flow and holding for 10 min for temperature-programmed desorption (TPD) of strongly adsorbed CO_2. Single-beam spectra, I, with a resolution of 4 cm^{-1} were obtained every 10 s, where each spectrum was averaged from 32 coadded scans.

RESULTS AND DICSUSSION

IR Spectra of Fresh Films. Figure 2 shows the IR absorbance spectra (log(1/I)) of TEPA films with thicknesses of 4, 10, and 20 μm in ATR and DRIFTS at 50 °C after pretreatment at 100 °C. The spectra of TEPA resembles those of organic amines which show the characteristic (i) asymmetric and symmetric N−H stretching bands at 3355 and 3284 $cm^{-1}$and N−H deformation band at 1595 cm^{-1} for primary amines, NH_2; (ii) asymmetric and symmetric C−H stretching bands at 2929 and 2809 cm^{-1}, C−H deformation band at 1456 cm^{-1}, and H−C−H twisting band at 1302 $cm^{-1}$and for CH_2; and (iii) C−N stretching band at 1125 cm^{-1} for $-CH_2-NH_2$.[40,41] The N−H stretching band of secondary amines, NH, is overlapped with that of the symmetrical stretching of NH_2.[41] The secondary amine band assignment for TEPA is further supported by the N−H stretching band observed at 3283 cm^{-1} for *N,N′*-dimethylethylenediamine.[42]

The ATR spectra of TEPA for different film thicknesses show nearly identical intensities and shapes for all bands,

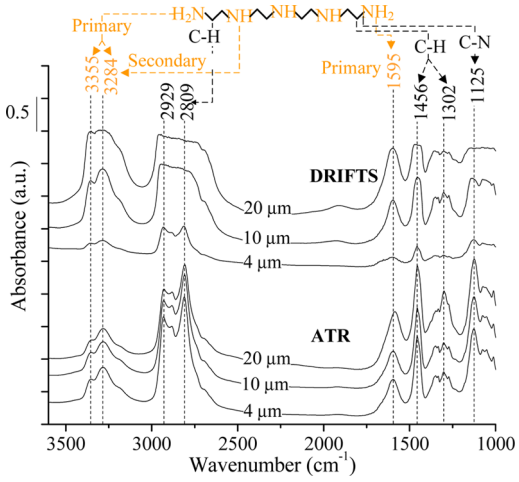

Figure 2. IR absorbance spectra of 4, 10, and 20 μm TEPA films at 50 °C in ATR and DRIFTS before CO_2 adsorption.

resulting from the same penetration depth of the IR beam into these various thickness films. The penetration depth is determined by the incident angle of the IR beam and the refractive indices of TEPA and the ZnSe ATR crystal (see the Supporting Information). In contrast, the DRIFTS spectra showed a significant variation in their intensities with film thickness. The 4 μm film has a low intensity ratio of N−H/C-H bands which could be attributed to the interaction between the metal surface and the N−H of TEPA. Increased N−H/C-H stretching (3355 and 3284 cm^{-1}/2929 cm^{-1}) and deformation (1595 cm^{-1}/1456 cm^{-1}) band intensity ratios with film thickness may be explained by the diminishing effect of the metal surface on TEPA at the top layers of the thicker films. Interestingly, the spectra show broadened N−H stretching bands with increased intensities from 4 to 20 μm thicknesses. These DRIFTS results were unexpected because the size of the TEPA molecule is less than 1.5 nm, which is 3 orders of magnitude less than the thickness of the TEPA films. The differences in the nature of adsorbed CO_2 near the film surface and within the bulk has only been observed by XPS at the nanometer scale.[36] We postulate that the broadened NH bands resulted from an increased number of amine−amine hydrogen bonds near the top layers of the 10 and 20 μm thick films. The presence of this hydrogen bonding would facilitate the formation of an interconnected network of ammonium-carbamate ion pairs. Furthermore, the hydrogen bonding near the films' surfaces would give a higher viscosity than that of the bulk, affecting the diffusion of the ion pairs. The flat C−H and N−H bands show that the detector was saturated because of the long IR path through the thicker films.

Although DRIFTS is not a good technique to study low viscosity liquid films, the absence of variations in the backgrounds of the TEPA film spectra, shown in Figure S6 in the Supporting Information, indicates that DRIFTS can serve as an excellent technique to study highly viscous films. We further demonstrated that the DRIFTS primarily observes the top surfaces of the amine films by depositing various thicknesses of TEPA onto a 4 μm poly(vinyl alcohol) (PVA) film. Figure S1 of the Supporting Information reveals that the IR features of PVA were nearly diminished by applying 12 μm of TEPA onto the PVA. The 12 μm depth is the DRIFTS detection limit for the amine film. By utilizing ATR and DRIFTS techniques, each with different penetration depths, we could study the structures

dx.doi.org/10.1021/am5031006 | ACS Appl. Mater. Interfaces 2014, 6, 13617−13626

Table 1. Average Molar Absorption Coefficients of Adsorbed CO_2 in the DRIFTS

IR band (cm^{-1})	assignment (species)	molar absorption coefficient ε_{Ads}[a] (σ, STD)(L $mmol^{-1}$ cm^{-1}) (%)
1575/1525	COO^-	0.052 (9.8)
1477	COO^-	0.047 (10.1)
1405	$NCOO^-$	0.033 (7.1)
1630	NH_3^+	0.034 (9.4)

[a]Average $\varepsilon_{Ads.}$ values were calculated for $c_{Ads.}$ values between 3.54 and 17.71 mmol of CO_2/g of TEPA.

and kinetics of adsorbed CO_2 at different locations within the TEPA film.

Calculation of Film CO_2 Capture Capacities. The molar absorption coefficients of adsorbed CO_2 ($\varepsilon_{Ads.}$), i.e., ammonium ions and carbamates, were determined by the detailed procedure in the Supporting Information, and are shown in Table 1. Beer's law, $c_{Ads=} A_{Ads}/(l_{TEPA}\varepsilon_{Ads})$,[43] was used to calculate the concentration of adsorbed CO_2 (capture capacity, c_{Ads}) for each film in DRIFTS from the following: (i) the IR path lengths through each TEPA film (l_{TEPA}, see the Supporting Information), (ii) the 1575/1525 cm^{-1} carbamate absorbance intensities (A_{Ads}) after CO_2 adsorption, and (iii) the corresponding ε_{Ads} value for 1575/1525 cm^{-1} from Table 1. The CO_2 capture capacities and amine efficiencies (CO_2/N) of the DRIFTS TEPA films are shown in Table 3.

Spectra of Adsorbed CO_2. Figure 3a shows the ATR absorbance spectra of adsorbed CO_2 on the TEPA films after

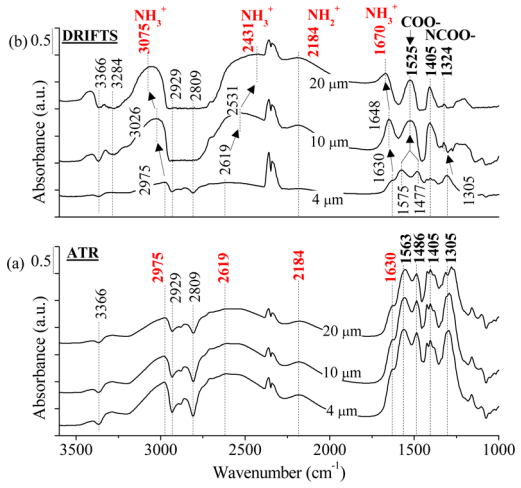

Figure 3. IR absorbance spectra of adsorbed CO_2 on 4, 10, and 20 μm TEPA films in (a) ATR and (b) DRIFTS modes after 10 min in a 15% CO_2/air flow. Absorbance = $\log(I_0/I)$, where I_0 was the single beam spectrum before CO_2 adsorption and I was the single beam spectrum during adsorption.

10 min in a 15%CO_2/air flow. The band assignments for adsorbed CO_2 species were reported in the literature and are tabulated in Table 2. Adsorption of CO_2 onto all TEPA films in ATR produced the characteristic (i) $NCOO^-$ skeletal vibration band at 1305 cm^{-1}, COO^- stretching bands at 1563 and 1486 cm^{-1}, and C−N stretching band at 1405 cm^{-1} for carbamates and (ii) NH_3^+ deformation and stretching bands at 1630 and 2975 cm^{-1}, respectively, for primary ammonium ions. The NH_3^+ was produced by proton transfer from the R-$NH_2^+COO^-$ intermediate to a neighboring R-NH_2 group, giving the negative 3366 cm^{-1} N−H band as illustrated in Scheme 1. The C−N stretching band for the resulting R-$NHCOO^-$ was observed at a

Table 2. IR Band Assignments for Adsorbed CO_2 Species

wavenumber (cm^{-1})	assignment	species	ref
3075−2975	NH_3^+ stretching	primary ammonium ions	30, 46
2750−1750	N−H combination	primary/secondary ammonium ions	30, 44, 45
1696	C═O	dimer carbamic acid	29, 30
1670−1630	NH_3^+ deformation	primary ammonium ions	29, 30, 46
1575−1525	COO^- stretching	carbamate	29, 30, 46
1486−1477	COO^- stretching	carbamate	30, 47
1405	C−N stretching/$NCOO^-$ skeletal vibration	carbamate	46, 48
1324−1305	$NCOO^-$ skeletal vibration	carbamate	30, 46, 47

lower wavenumber than that for a TEPA/silica sorbent,[30] suggesting weaker binding of CO_2 to NH_2 in a liquid amine environment.

The N−H···N−H hydrogen bonding of ammonium ions produced the broad N−H bands between 2750 and 1750 cm^{-1}, with a maximum intensity at 2619 cm^{-1} for primary ammonium ion species, NH_3^+. These broad N−H bands are a combination of deformation and stretching vibrations. The NH_3^+ could also be formed by deprotonation of R-NH^+COO^--R by NH_2 of the same TEPA molecule to form ammonium/carbamate zwitterions. The broad band at 2184 cm^{-1} is tentatively assigned to the N−H combination bands of secondary ammonium ions, NH_2^+, which were produced by deprotonation of R-NH^+COO^- by secondary amines. A general trend for NH_2^+ giving lower wavenumber bands than NH_3^+ can be observed for various organic amine salts.[44] The assignment of NH_2^+ for TEPA is further supported by weak combination bands specifically reported at 2140 and 2160 cm^{-1} for piperazine hydrochloride and dimethylamine hydrochloride, respectively.[45]

The band intensities of the carbamate at 1563 cm^{-1} (1.3) and ammonium ion at 1630 cm^{-1} (0.7) for the 20 μm film were 23 and 33% less, respectively, than those for 4 μm, reflecting lower concentration of adsorbed CO_2 at the bottom layers of the thicker film. Although the liquid TEPA molecules can move between different layers of the films, the observation of a concentration gradient of the ammonium-carbamate ion pairs suggests that these ion pairs undergo very slow diffusion from the top to the bottom of the film by facilitated transport. The low adsorbed CO_2 concentration for the thicker film could be correlated with lower uptake of PEI/silica sorbents containing longer pores (24−40 μm) than those containing shorter pores (0.2 μm),[49] which was attributed to high CO_2 diffusion resistance through more amine layers. Interestingly, the ATR spectra of adsorbed CO_2 resembles the DRIFTS spectra for low concentration of adsorbed CO_2 on the 4 μm film at 0.1 min

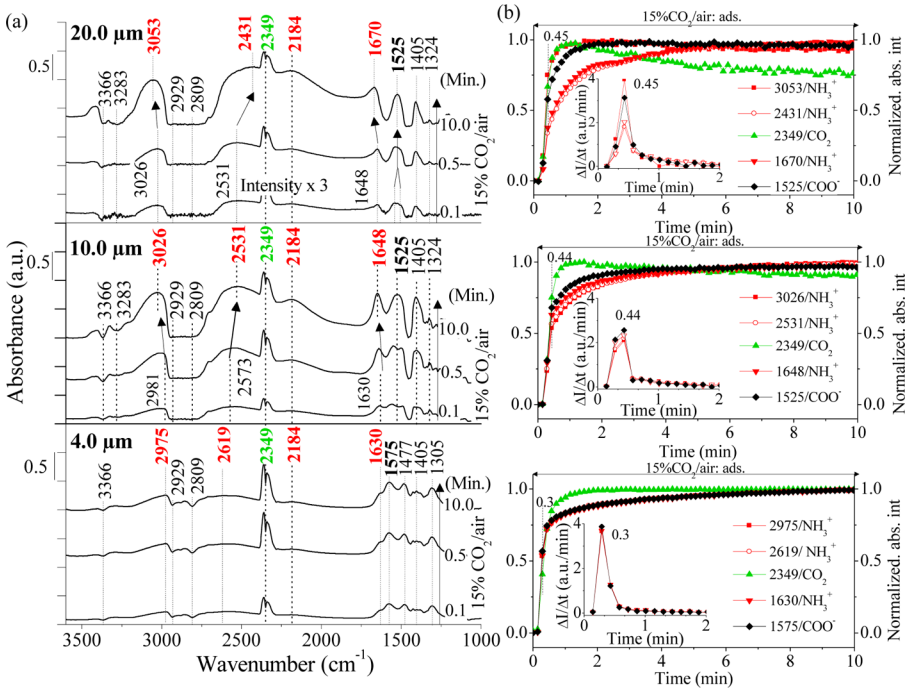

Figure 4. (a) IR absorbance spectra of adsorbed CO_2 on the TEPA films in DRIFTS mode during CO_2 adsorption and (b) normalized IR absorbance intensity profiles of adsorbed and gas-phase CO_2. The insets of b show the relative rates of CO_2 adsorption ($\Delta I/\Delta t$) onto each film as a function of time. Norm. abs. int. = $(I_t - I_{min})/(I_{max} - I_{min})$, where I_t is the absorbance intensity at time t for the profile of interest, I_{max} is the maximum profile intensity, and I_{min} is the minimum profile intensity.

(Figure 4a), where the surface amine layers were exposed to low CO_2 partial pressure upon switching to the CO_2/air flow.

The DRIFTS spectrum of adsorbed CO_2 on the 4 μm film in Figure 3b exhibited shifts in the carbamate band positions and a reduced 2619 cm^{-1}/2975 cm^{-1} intensity ratio compared to those in the ATR spectrum. These results suggest diminished hydrogen bonding of ammonium-carbamate species with the reduced available NH_2 near the TEPA/metal interface. In other words, NH_2 groups interacting with metal are unable to further stabilize adsorbed CO_2. The negative NH_2 band at 3366 cm^{-1} indicates that the adsorbed CO_2 was associated more with primary than secondary amines throughout the thinnest film. Intramolecular proton transfer of the R-$NH_2^+COO^-$ intermediate could produce NHCOOH (carbamic acid) at the top layers of the TEPA film, and has been observed within 9 nm of a CO_2/ionic liquid (NH_2) film interface by XPS.[35] Carbamic acid was not observed on TEPA because of complete penetration of the DRIFTS IR beam into the film. The calculated CO_2 capture capacity of 10.7 mmol CO_2/g-TEPA results in an amine efficiency of 0.40 mol CO_2/mol N, shown in Table 3, which is close to the theoretical 0.5 value for ammonium-carbamate formation and shows effective utilization of surface and bulk amine sites to adsorb CO_2.

Increasing the TEPA film thickness increased the intensity ratio of the 2750−1750 cm^{-1}/1750−1000 cm^{-1} region and shifted/merged the carbamate bands, suggesting enhanced CO_2 adsorption onto secondary amines.[30] Proton transfer from the R-NH^+COO^--R intermediate to neighboring amines generated the negative NH band at 3284 cm^{-1}, shifted the positions of the ammonium ion bands, and produced more prominent features for NH_2^+ at 2184 cm^{-1} than NH_3^+ at 2531 cm^{-1}.

Table 3. CO_2 Capture Capacities and Amine Efficiencies of the TEPA Films in DRIFTS

film thickness (μm)	CO_2 capture capacity (mmol of CO_2/g of TEPA)	amine efficiency (CO_2/N)
4	10.7	0.40
10	7.1	0.27
20	3.8	0.14 (max.)

These results indicate more association of NH in the surface regions of the thicker than thinner films in forming ammonium-carbamate ion pairs and zwitterions. We further speculate a higher availability of NH_2 sites at the surface compared to the bulk for deprotonation of R-$NH_2^+COO^-$ intermediates, converting the amine sites into ammonium ions. CO_2 adsorption onto 15 and 50 wt % polyethylenimine (PEI)/SBA-15[46] (0.2 and 1.0 nm of amine) produced similar IR features for ammonium-carbamate species as those for 4 and 10 μm TEPA films. These results suggest that the CO_2 adsorption mechanisms for liquid amine films can be used to explain the behavior of immobilized amine layers.

The amine efficiencies of the 10 and 20 μm films were 40 and 65% lower, respectively, than that for the 4 μm film. The lower amine efficiencies for the thicker films confirm that adsorbed CO_2 at the films' surfaces caused diffusion limitations, which restricted the access of CO_2 to available bulk amine sites. The adsorbed species are stabilized by hydrogen bonding with neighboring amines to form an interconnected network,[34] which slowed CO_2 diffusion to the bulk amine groups. The formation of an interconnected network, in part by NH, could increase the viscosity of the liquid amine or ever form a gel at the TEPA film surface.[50] Quantum chemistry calculations revealed higher binding energy of CO_2 to the NH (20.4 kJ/mol) than NH_2 (14.5 kJ/mol) groups of TEPA,[18] suggesting that slow CO_2 diffusion through the surface network occurred mainly by solution-diffusion (gas-phase) rather than facilitated transport across the NH sites. A high CO_2 binding energy to

dx.doi.org/10.1021/am5031006 | ACS Appl. Mater. Interfaces 2014, 6, 13617−13626

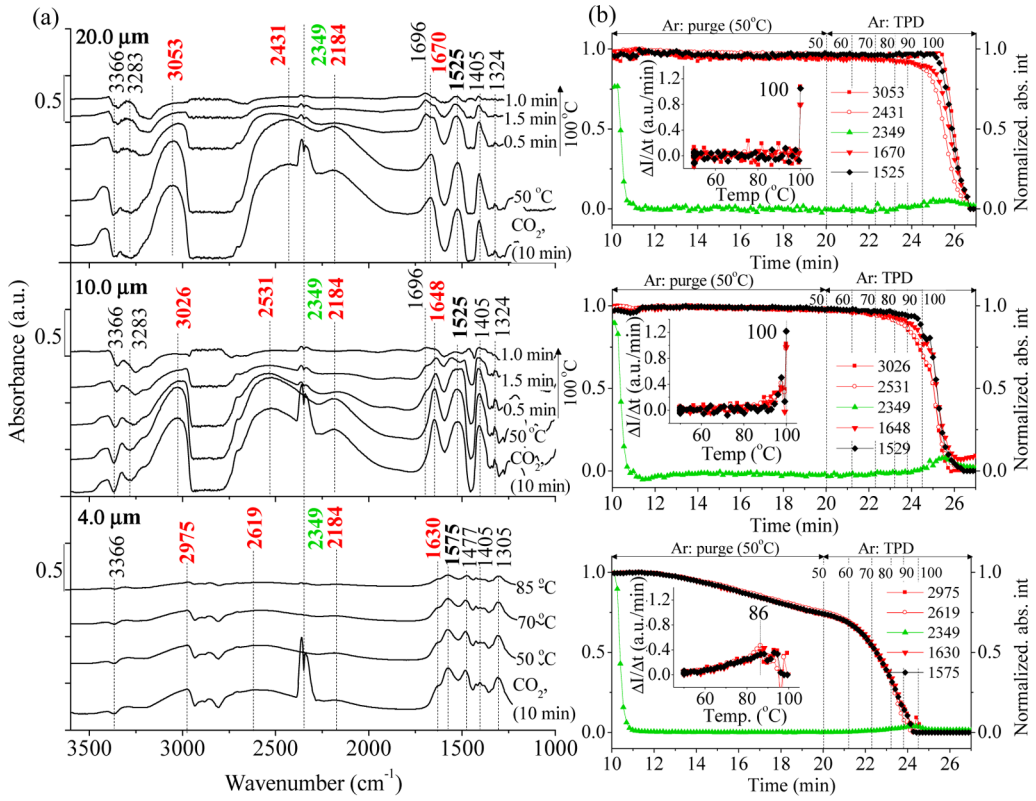

Figure 5. (a) IR absorbance spectra of adsorbed CO_2 after Ar purge and during TPD, and (b) normalized IR intensity profiles of adsorbed and gas-phase CO_2. The insets of b show the relative rates of CO_2 desorption from each film as a function of temperature.

-NH (secondary amine functional group) is in contrast to the low energy observed elsewhere experimentally.[51] This discrepancy can be explained by the presence of more hydrogen bonding of the ion pairs associated with neighboring secondary amine groups, which was observed near our film surfaces. Diminished CO_2/N efficiency for TEPA/SBA-15 with increased amine loading[15] further supports limited CO_2 diffusion through more amine layers.

Interestingly, the formation of the interconnected surface network is associated with the high degree of amine−amine hydrogen bonding of the films before adsorption. In other words, the mechanism for CO_2 adsorption onto amine films could be predicted by the DRIFTS spectra of the fresh films.

CO_2 Adsorption in DRIFTS. Figure 4a compares the DRIFTS absorbance spectra of adsorbed CO_2 as a function of time on 3 different thickness films. The spectra of adsorbed CO_2 on the 4 μm film show identical features for band positions and shapes with increasing intensity, indicating a homogeneous distribution of surface and bulk species. The spectra of adsorbed CO_2 for the 10 and 20 μm films show an appreciable difference in the IR band intensity growth. The spectrum at 0.1 min, which represents adsorbed CO_2 on primary amines at low concentration, resembled that obtained for 4 μm. As CO_2 exposure time increases, the growth of NH_3^+ and NH_2^+ ammonium ion band intensities at 2431 and 2184 cm^{-1} and the shifted/merged carbamate bands suggest further association of adsorbed CO_2 with secondary amines.

Figure 4b plots the intensities of ammonium ion and carbamate bands with time while flowing CO_2/air. The ammonium ion and carbamate intensities increased at the same rate on the 4 μm film, compared to leading of the ammonium ion profile relative for that for carbamate for the 10 and 20 μm films. The NH_2^+ band around 2184 cm^{-1}emerged at 0.5 min on these thicker films. The adsorbed CO_2 spectra and intensity profiles suggest two possible pathways for ammonium ion formation: (i) CO_2 adsorption onto NH_2 sites first to produce primary NH_3^+- $NHCOO^-$ ion pairs and then onto the NH sites or (ii) migration of an NH_3^+ proton to NH for regeneration of the NH_2 to adsorbed incoming CO_2. The migration of these protons is diffusion limited, evidenced by the increased lag between the ammonium ion and carbamate profiles with film thickness.

The kinetics of CO_2 adsorption onto immobilized amine sorbents have been quantified by the rate constants (k) by fitting the CO_2 uptake curves to various models, including the linear driving force (LDF),[52] first and second order Lagergen,[53] fractional order,[15] and Avrami.[53,54] The use of the various models in the literature makes the comparison of adsorption kinetics challenging. We found that adsorption half time, which is defined as the time required for the sorbents to reach half of their saturated adsorption capacities, can serve as a semi-quantitative indicator of the overall adsorption and diffusion kinetics.[55,56] Analysis of the CO_2 profiles for amine sorbents in the literature[52,54,55,57] revealed that the sorbents' adsorption half times were within the range of those of our TEPA films, between 0.28 and 0.42 min.[52,54,55,57] Comparable adsorption half times for the sorbents and films suggests similar adsorption kinetics for immobilized and liquid amines, in spite of potential diffusion effects in the immobilized amine sorbent. Furthermore, the adsorbed CO_2 on immobilized and liquid amines are similar.

The derivative intensity profiles of the adsorbed species ($\Delta I/\Delta t$) for 4 μm, shown in the inset, increased sharply up to a maximum relative rate of $\Delta I/\Delta t$ = 4.0 au/min at 0.3 min, and

dx.doi.org/10.1021/am5031006 | ACS Appl. Mater. Interfaces 2014, 6, 13617−13626

then symmetrically decreased until 1 min. These results confirm negligible CO_2 diffusion limitations through the entire film. In contrast, the $\Delta I/\Delta t$ profiles for the 10 and 20 μm films rapidly increased to maximum relative rates of 2.5 and 1.8−4.0 au/min around 0.45 min, respectively, and then steadily decreased until 2.0 min. These asymmetrical intensity profiles reveal slow CO_2 diffusion through the interconnected surface network and to the bulk amines. Asymmetrical CO_2 uptake profiles for amine/silica sorbents[27,46] have been attributed to fast adsorption onto external amine layers followed by slow diffusion into bulk layers. It was further postulated that slow bulk diffusion resulted from the formation of an ionic carbamate gel at the amine surface layers.[58]

CO_2 Desorption in DRIFTS. Figure 5a shows the DRIFTS absorbance spectra of adsorbed CO_2 after Ar purge and during TPD from the TEPA films. Reducing the partial pressure of CO_2 by switching to the Ar flow at 50 °C desorbed about 20% of the adsorbed CO_2 from the 4 μm film, evidenced by the reduced carbamate and ammonium ion band intensities. These species desorbed at zero CO_2 partial pressure and constant temperature are considered as weakly adsorbed CO_2.

CO_2 desorption kinetics have been compared by examining the decay curves of adsorbed CO_2.[30] This type of decay curve has been further quantified by fitting to the Avrami equation.[59] Comparison of the COO^- carbamate decay curve during CO_2 desorption from the 4 μm TEPA film, shown in Figure 4b, with that of a high amine density sorbent (34.50 N atoms (TEPA)/nm^2)[60] indicates that adsorbed CO_2 desorbs from the films and sorbents within the same time scale. These results are in contrast to those of the thicker films.

Increasing the temperature of the 4 μm film accelerated the removal of the adsorbed CO_2, beginning at 60 °C. The spectra during desorption resembles those during adsorption, further supporting that the adsorbed species were reversibly adsorbed to the amine groups.

In contrast to the 4 μm film, adsorbed CO_2 on the 10 and 20 μm films required a higher desorption temperature (100 °C) than that of 4 μm. Higher desorption temperature for the thicker films shows stronger binding of the ion pairs and zwitterions to NH groups that comprise the hydrogen bonded surface network. The IR features of adsorbed CO_2 being desorbed at 100 °C resemble those at 0.1 min of CO_2 adsorption (Figure 4a), suggesting the removal of bulk species associated with primary amines trapped beneath the network.

Figure 5b shows increased lead times of the ammonium ion profiles relative to the carbamate profiles with increased film thickness during thermal desorption. It is interesting to observe the reversed lead-lag trend for the ammonium and carbamate ion profiles when comparing with those for adsorption in Figure 4b. Faster reduction of the ammonium ion than carbamate profiles suggests that deprotonation precedes the decomposition of carbamate during CO_2 desorption.

The thermally desorbed CO_2 can be considered as a strongly adsorbed species. The key differences in the IR spectra between strongly and weakly adsorbed CO_2 are the intensities of ammonium ions and the variations in the carbamate bands. These differences can be, in part, attributed to the availability of -NH_2/NH sites for protonation, especially -NH_2. The high fraction of the NH_2, primary amines, on TEPA interacting with the metal surface for the 4 μm film would produce more weakly adsorbed CO_2 than the high fraction of available primary amine sites for the 10 and 20 μm films. It is likely that a high fraction of carbamate on the 4 μm film near the TEPA/metal interface is associated with the secondary amine sites.

The 10 and 20 μm films exhibited slow reduction in the 2531 and 2431 cm^{-1} ammonium ion profiles beginning at 65 °C prior to CO_2 desorption, which could result from dissociation of ionic hydrogen bonds (IHB) between ammonium ions and NH_2/NH. A reported lower IHB strength of 86.8 kJ/mol for $CH_3NH_3^+\cdots H_2NCH_3$ (gas-phase)[61] than a 155−45 kJ/mol CO_2 binding strength for silica-immobilized aminopropylsilane (APS)[62] further supports this hypothesis.

The higher fraction of weakly adsorbed ammonium ion and carbamate species on the thinner 4 μm film gave the broad $\Delta I/\Delta t$ profiles with respect to temperature, reflecting a wide distribution of CO_2-amine binding strengths throughout the film. In contrast, the higher fraction of strongly adsorbed species comprising the surface network of the 10 and 20 μm films gave narrower $\Delta I/\Delta t$ profiles, which showed faster CO_2 desorption kinetics at higher temperature.

Figure 6 compares the intensity profiles of ATR (1563 cm^{-1}) and DRIFTS (1575, 1525 cm^{-1}) for COO^- during TPD.

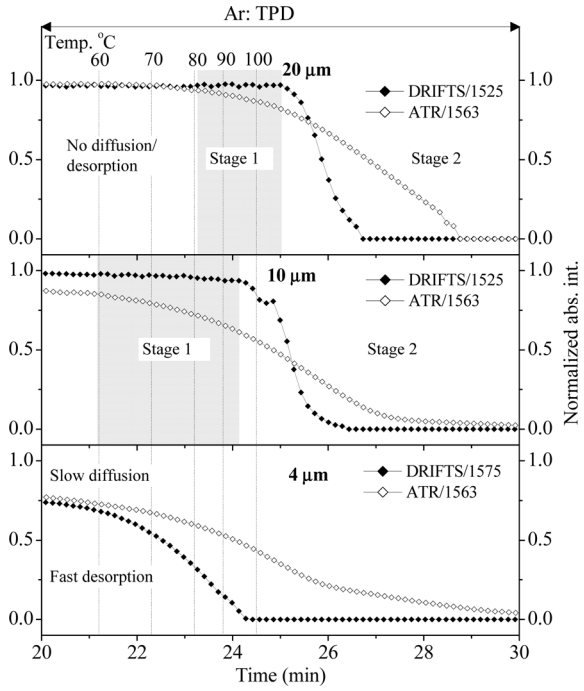

Figure 6. Normalized DRIFTS and ATR absorbance intensity profiles of carbamate (COO^-) during TPD. The time scales of the ATR profiles were offset by 0.7 min relative to those for DRIFTS to account for the different heating rates of the IR accessories.

Slower decay in the 1577/1525 cm^{-1} carbamate ATR profile than that of DRIFTS for the 4 μm film indicates that weakly adsorbed CO_2 removal was limited by the slow rate of facilitated transport/diffusion through the bulk amines. Increasing the TEPA film thickness inhibited bulk diffusion and delayed surface desorption of strongly adsorbed CO_2, which are evidenced by the slow responses in the respective ATR and DRIFTS profiles. Note that ATR observed the adsorbed species at the bottom of the film which is near the surface of the ZnSe window. Desorption of strongly adsorbed CO_2 from the thicker films likely occurred in two stages: (i) slow facilitated transport process via the formation and decomposition of primary ammonium-carbamate species, as

shown by the ATR curves in Figure 6 followed by (ii) rapid surface desorption of primary and secondary ammonium-carbamate species at 100 °C, as shown by the DRIFTS profiles. At 100 °C, the surface network of ammonium-carbamate species was eliminated, which liberated bulk CO_2. The flat ATR and DRIFTS carbamate profiles for the 20 μm film up to 80 °C reveal the inability of adsorbed CO_2 to desorb from the thick, strongly bound surface network at a lower temperature.

CONCLUSIONS

The adsorption and desorption of CO_2 for different thicknesses of TEPA films were studied by in situ ATR and DRIFTS techniques under transient conditions. The IR results showed that CO_2 adsorbed onto the 4 μm film as ammonium-carbamate ion pairs and zwitterions, which rapidly diffused into the bulk. Increasing the film thickness to 20 μm resulted in a thick, interconnected surface network of strongly adsorbed species. This network contained a high concentration of ammonium ions and slowed down CO_2 gas diffusion into and diminished access of the bulk amine groups, reducing the CO_2/N efficiency by a minimum of 65%. The corresponding ATR spectra of thick TEPA films confirmed the low concentration of adsorbed CO_2 within the bulk due to diffusion limitations. TPD studies showed that weakly adsorbed CO_2, of which the IR spectra exhibited low intensity of ammonium ions, were released from the 4 μm film beginning at 50 °C by decreasing the CO_2 partial pressure through flowing Ar. Desorption of adsorbed CO_2 from the thicker films could occur in two stages: (i) slow facilitated transport processes via the formation and decomposition of primary ammonium-carbamate species followed by (ii) elimination of the ammonium-carbamate surface network at 100 °C for rapid desorption of CO_2. These results show that diffusion, as well as binding strength, play a key role for CO_2 adsorption/desorption onto/from thick amine films. Faster CO_2 mass transfer and higher amine efficiencies for sorbents can be achieved by using thinner layers of immobilized amines on the porous support. The ATR and DRIFTS techniques presented in this study can also be used to examine the nature of adsorbed CO_2 on viscous films prepared from different amines.

ASSOCIATED CONTENT

Supporting Information

Additional figures as stated in the text. This material is available free of charge via the Internet at http://pubs.acs.org.

AUTHOR INFORMATION

Corresponding Author

*E-mail: schuang@uakron.edu. Tel.: +1 330.972.6993. Fax: +1 330.972.5290.

Present Address

‡C.S.S. is currently at Monash University, Victoria 3800, Australia

Funding

This work is supported by the U.S. Department of Energy under Grant DE-FE0001780.

Notes

The authors declare no competing financial interest.

ACKNOWLEDGMENTS

We thank Miss Uma Tumuluri for her help in collecting IR data for determining the DRIFTS penetration depth and Miss Jie Yu for collecting transmission IR data for determining the CO_2 gas molar absorption coefficient.

REFERENCES

(1) Keeling, C. D.; Piper, S. C.; Bacastow, R. B.; Wahlen, M.; Whorf, T. P.; Heimann, M.; Meijer, H. A. *Exchanges of Atmospheric CO_2 and $^{13}CO_2$ with the Terrestrial Biosphere and Oceans from 1978 to 2000. I. Global Aspects*; SIO Reference Series no. 01-06; Scripps Institute of Oceanography: San Diego, CA, 2001; p 88.

(2) Usubharatana, P.; Tontiwachwuthikul, P. Enhancement Factor and Kinetics of CO_2 Capture by MEA-methanol Hybrid Solvents. *Energy Proc.* **2009**, *1* (1), 95−102.

(3) Mangalapally, H. P.; Notz, R.; Hoch, S.; Asprion, N.; Sieder, G.; Garcia, H.; Hasse, H. Pilot Plant Experimental Studies of Post Combustion CO_2 Capture by Reactive Absorption with MEA and New Solvents. *Energy Proc.* **2009**, *1* (1), 963−970.

(4) Freguia, S.; Rochelle, G. T. Modeling of CO_2 Capture by Aqueous Monoethanolamine. *AIChE J.* **2003**, *49* (7), 1676−1686.

(5) Abu-Zahra, M. R. M.; Schneiders, L. H. J.; Niederer, J. P. M.; Feron, P. H. M.; Versteeg, G. F. CO_2 Capture from Power Plants: Part I. A Parametric Study of the Technical Performance Based on Monoethanolamine. *Int. J. Greenhouse Gas Control* **2007**, *1* (1), 37−46.

(6) Kuntz, J.; Aroonwilas, A. Mass-transfer Efficiency of a Spray Column for CO_2 Capture by MEA. *Energy Proc.* **2009**, *1* (1), 205−209.

(7) Ciftja, A. F.; Hartono, A.; Svendsen, H. F. ^{13}C NMR as a Method Species Determination in CO2 absorbent systems. *Int. J. Greenhouse Gas Control* **2013**, *16* (0), 224−232.

(8) Xie, H.-B.; He, N.; Song, Z.; Chen, J.; Li, X. Theoretical Investigation on the Different Reaction Mechanisms of Aqueous 2-Amino-2-methyl-1-propanol and Monoethanolamine with CO_2. *Ind. Eng. Chem. Res.* **2014**, DOI: 10.1021/ie403280h.

(9) Alper, E. Reaction Mechanism and Kinetics of Aqueous Solutions of 2-amino-2-methyl-1-propanol and Carbon Dioxide. *Ind. Eng. Chem. Res.* **1990**, *29* (8), 1725−1728.

(10) Xie, Q.; Aroonwilas, A.; Veawab, A. Measurement of Heat of CO_2 Absorption into 2-Amino-2-methyl-1-propanol (AMP)/Piperazine (PZ) Blends Using Differential Reaction Calorimeter. *Energy Proc.* **2013**, *37* (0), 826−833.

(11) Saravanamurugan, S.; Kunov-Kruse, A. J.; Fehrmann, R.; Riisager, A. Amine-Functionalized Amino Acid-based Ionic Liquids as Efficient and High-Capacity Absorbents for CO_2. *ChemSusChem* **2014**, *7* (3), 897−902.

(12) Wang, X.; Akhmedov, N. G.; Duan, Y.; Luebke, D.; Hopkinson, D.; Li, B. Amino Acid-Functionalized Ionic Liquid Solid Sorbents for Post-Combustion Carbon Capture. *ACS Appl. Mater. Interfaces* **2013**, *5* (17), 8670−8677.

(13) Luo, X. Y.; Ding, F.; Lin, W. J.; Qi, Y. Q.; Li, H. R.; Wang, C. M. Efficient and Energy-Saving CO_2 Capture through the Entropic Effect Induced by the Intermolecular Hydrogen Bonding in Anion-Functionalized Ionic Liquids. *J. Phys. Chem. Lett.* **2014**, *5* (2), 381−386.

(14) Kasahara, S.; Kamio, E.; Otani, A.; Matsuyama, H. Fundamental Investigation of the Factors Controlling the CO_2 Permeability of Facilitated Transport Membranes Containing Amine-Functionalized Task-Specific Ionic Liquids. *Ind. Eng. Chem. Res.* **2014**, *53* (6), 2422−2431.

(15) Zhao, A.; Samanta, A.; Sarkar, P.; Gupta, R. Carbon Dioxide Adsorption on Amine-Impregnated Mesoporous SBA-15 Sorbents: Experimental and Kinetics Study. *Ind. Eng. Chem. Res.* **2013**, *52* (19), 6480−6491.

(16) Yao, M.; Dong, Y.; Hu, X.; Feng, X.; Jia, A.; Xie, G.; Hu, G.; Lu, J.; Luo, M.; Fan, M. Tetraethylenepentamine-Modified Silica Nanotubes for Low-Temperature CO_2 Capture. *Energy Fuels* **2013**, *27* (12), 7673−7680.

(17) De Canck, E.; Ascoop, I.; Sayari, A.; Van Der Voort, P. Periodic Mesoporous Organosilicas Functionalized with a Wide Variety of Amines for CO_2 Adsorption. *Phys. Chem. Chem. Phys.* **2013**, *15* (24), 9792−9799.

(18) Wang, X.; Li, H.; Hou, X.-J. Amine-Functionalized Metal Organic Framework as a Highly Selective Adsorbent for CO_2 over CO. *J. Phys. Chem. C* **2012**, *116* (37), 19814−19821.
(19) Isenberg, M.; Chuang, S. S. C. The Nature of Adsorbed CO_2 and Amine Sites on the Immobilized Amine Sorbents Regenerated by Industrial Boiler Steam. *Ind. Eng. Chem. Res.* **2013**, *52* (35), 12530−12539.
(20) Vieira, R. B.; Pastore, H. O. Polyethylenimine-Magadiite Layered Silicate Sorbent for CO_2 Capture. *Environ. Sci. Technol.* **2014**, *48* (4), 2472−2480.
(21) Chen, Z.; Deng, S.; Wei, H.; Wang, B.; Huang, J.; Yu, G. Polyethylenimine-Impregnated Resin for High CO_2 Adsorption: An Efficient Adsorbent for CO_2 Capture from Simulated Flue Gas and Ambient Air. *ACS Appl. Mater. Interfaces* **2013**, *5* (15), 6937−6945.
(22) Rezaei, F.; Lively, R. P.; Labreche, Y.; Chen, G.; Fan, Y.; Koros, W. J.; Jones, C. W. Aminosilane-Grafted Polymer/Silica Hollow Fiber Adsorbents for CO2 Capture from Flue Gas. *ACS Appl. Mater. Interfaces* **2013**, *5* (9), 3921−3931.
(23) Li, W.; Bollini, P.; Didas, S. A.; Choi, S.; Drese, J. H.; Jones, C. W. Structural Changes of Silica Mesocellular Foam Supported Amine-Functionalized CO_2 Adsorbents Upon Exposure to Steam. *ACS Appl. Mater. Interfaces* **2010**, *2* (11), 3363−3372.
(24) Monazam, E. R.; Spenik, J.; Shadle, L. J. CO_2 Desorption Kinetics for Immobilized Polyethylenimine (PEI). *Energy Fuels* **2014**, *28* (1), 650−656.
(25) Fauth, D. J.; Gray, M. L.; Pennline, H. W.; Krutka, H. M.; Sjostrom, S.; Ault, A. M. Investigation of Porous Silica Supported Mixed-Amine Sorbents for Post-Combustion CO_2 Capture. *Energy Fuels* **2012**, *26* (4), 2483−2496.
(26) Chang, F.-Y.; Chao, K.-J.; Cheng, H.-H.; Tan, C.-S. Adsorption of CO_2 onto amine-grafted mesoporous silicas. *Sep. Purif. Technol.* **2009**, *70* (1), 87−95.
(27) Sanz, R.; Calleja, G.; Arencibia, A.; Sanz-Pérez, E. S. CO_2 Uptake and Adsorption Kinetics of Pore-Expanded SBA-15 Double-Functionalized with Amino Groups. *Energy Fuels* **2013**, *27* (12), 7637−7644.
(28) Danckwerts, P. V. The Reaction of CO_2 with Ethanolamines. *Chem. Eng. Sci.* **1979**, *34* (4), 443−446.
(29) Bacsik, Z. n.; Ahlsten, N.; Ziadi, A.; Zhao, G.; Garcia-Bennett, A. E.; Martín-Matute, B. n.; Hedin, N. Mechanisms and Kinetics for Sorption of CO_2 on Bicontinuous Mesoporous Silica Modified with n-Propylamine. *Langmuir* **2011**, *27* (17), 11118−11128.
(30) Chakravartula Srivatsa, S.; Chuang, S. S. C. Infrared Study of Strongly and Weakly Adsorbed CO_2 on Fresh and Oxidative Degraded Amine Sorbents. *J. Phys. Chem. C* **2013**, *117* (18), 9196−9205.
(31) Francisco, G. J.; Chakma, A.; Feng, X. Membranes Comprising of Alkanolamines Incorporated into Poly(vinyl alcohol) Matrix for CO_2/N_2 Separation. *J. Membr. Sci.* **2007**, *303* (1−2), 54−63.
(32) Cussler, E. L.; Aris, R.; Bhown, A. On the Limits of Facilitated Diffusion. *J. Membr. Sci.* **1989**, *43* (2−3), 149−164.
(33) Mebane, D. S.; Kress, J. D.; Storlie, C. B.; Fauth, D. J.; Gray, M. L.; Li, K. Transport, Zwitterions, and the Role of Water for CO_2 Adsorption in Mesoporous Silica-Supported Amine Sorbents. *J. Phys. Chem. C* **2013**, *117* (50), 26617−26627.
(34) Wilfong, W. C.; Chuang, S. S. C. Probing the Adsorption/Desorption of CO_2 on Amine Sorbents by Transient Infrared Studies of Adsorbed CO_2 and C_6H_6. *Ind. Eng. Chem. Res.* **2014**, DOI: 10.1021/ie404403q.
(35) Niedermaier, I.; Bahlmann, M.; Papp, C.; Kolbeck, C.; Wei, W.; Krick Calderón, S.; Grabau, M.; Schulz, P. S.; Wasserscheid, P.; Steinrück, H.-P.; Maier, F. Carbon Dioxide Capture by an Amine Functionalized Ionic Liquid: Fundamental Differences of Surface and Bulk Behavior. *J. Am. Chem. Soc.* **2014**, *136* (1), 436−441.
(36) Lewis, T.; Faubel, M.; Winter, B.; Hemminger, J. C. CO_2 Capture in Amine-Based Aqueous Solution: Role of the Gas−Solution Interface. *Angew. Chem., Int. Ed.* **2011**, *50* (43), 10178−10181.
(37) Liu, Q.; Shi, Y.; Zheng, S.; Ning, L.; Ye, Q.; Tao, M.; He, Y. Amine-functionalized Low-cost Industrial Grade Multi-walled Carbon Nanotubes for the Capture of Carbon Dioxide. *J. Energy Chem.* **2014**, *23* (1), 111−118.
(38) Zhao, W.; Zhang, Z.; Li, Z.; Cai, N. Investigation of Thermal Stability and Continuous CO2 Capture from Flue Gases with Supported Amine Sorbent. *Ind. Eng. Chem. Res.* **2013**, *52* (5), 2084−2093.
(39) Feng, X.; Hu, G.; Hu, X.; Xie, G.; Xie, Y.; Lu, J.; Luo, M. Tetraethylenepentamine-Modified Siliceous Mesocellular Foam (MCF) for CO2 Capture. *Ind. Eng. Chem. Res.* **2013**, *52* (11), 4221−4228.
(40) Miller, Duane D. In Situ Infrared Study of G-S/L-S Adsorption and Photocatalytic Processes. *Ph.D. Dissertation*, University of Akron, Akron, OH, 2009.
(41) Spell, H. L. Determination of Piperazine Rings in Ethyleneamines, Poly(ethyleneamine), and Polyethylenimine by Infrared Spectrometry. *Anal. Chem.* **1969**, *41* (7), 902−905.
(42) McDonald, T. M.; D'Alessandro, D. M.; Krishna, R.; Long, J. R. Enhanced Carbon Dioxide Capture Upon Incorporation of N,N[prime or minute]-dimethylethylenediamine in the Metal-organic Framework CuBTTri. *Chem. Sci.* **2011**, *2* (10), 2022−2028.
(43) Griffiths, P. R.; de Haseth, J. A. *Fourier Transform Infrared Spectroscopy*, second ed.; John Wiley & Sons: Hoboken, NJ, 2007; pp 1−529.
(44) Colthup, N. B.; Daly, L. H.; Wiberley, S. E. *Introduction to Infrared and Raman Spectroscopy*, second ed.; Academic Press: New York, 1975; pp 1−523.
(45) Heacock, R. A.; Marion, L. The Infrared Spectra of Secondary Amines and Their Salts. *Can. J. Chem.* **1956**, *34* (12), 1782−1795.
(46) Wang, X.; Schwartz, V.; Clark, J. C.; Ma, X.; Overbury, S. H.; Xu, X.; Song, C. Infrared Study of CO_2 Sorption over "Molecular Basket" Sorbent Consisting of Polyethylenimine-Modified Mesoporous Molecular Sieve. *J. Phys. Chem. C* **2009**, *113* (17), 7260−7268.
(47) Bacsik, Z. n.; Atluri, R.; Garcia-Bennett, A. E.; Hedin, N. Temperature-Induced Uptake of CO_2 and Formation of Carbamates in Mesocaged Silica Modified with n-Propylamines. *Langmuir* **2010**, *26* (12), 10013−10024.
(48) Silverstein, R. M.; Webster, F. X.; Kiemle, D. *Spectrometric Identification of Organic Compounds*; John Wiley & Sons: Hoboken, NJ, 2005; pp 1−502.
(49) Heydari-Gorji, A.; Yang, Y.; Sayari, A. Effect of the Pore Length on CO_2 Adsorption over Amine-Modified Mesoporous Silicas. *Energy Fuels* **2011**, *25* (9), 4206−4210.
(50) Rudkevich, D. M.; Xu, H. Carbon Dioxide and Supramolecular Chemistry. *Chem. Commun.* **2005**, *21*, 2651−2659.
(51) Ko, Y. G.; Shin, S. S.; Choi, U. S. Primary, Secondary, and Tertiary Amines for CO_2 Capture: Designing for Mesoporous CO_2 Adsorbents. *J. Colloid Interface Sci.* **2011**, *361* (2), 594−602.
(52) Monazam, E. R.; Shadle, L. J.; Siriwardane, R. Performance and Kinetics of a Solid Amine Sorbent for Carbon Dioxide Removal. *Ind. Eng. Chem. Res.* **2011**, *50* (19), 10989−10995.
(53) Heydari-Gorji, A.; Sayari, A. CO_2 Capture on Polyethylenimine-impregnated Hydrophobic Mesoporous Silica: Experimental and Kinetic Modeling. *Chem. Eng. J.* **2011**, *173* (1), 72−79.
(54) Serna-Guerrero, R.; Sayari, A. Modeling Adsorption of CO_2 on Amine-functionalized Mesoporous Silica. 2: Kinetics and breakthrough curves. *Chem. Eng. J.* **2010**, *161* (1−2), 182−190.
(55) Tanthana, J.; Chuang, S. S. C. In Situ Infrared Study of the Role of PEG in Stabilizing Silica-Supported Amines for CO_2 Capture. *ChemSusChem* **2010**, *3* (8), 957−964.
(56) Liu, F.-Q.; Wang, L.; Huang, Z.-G.; Li, C.-Q.; Li, W.; Li, R.-X.; Li, W.-H. Amine-Tethered Adsorbents Based on Three-Dimensional Macroporous Silica for CO_2 Capture from Simulated Flue Gas and Air. *ACS Appl. Mater. Interfaces* **2014**, *6* (6), 4371−4381.
(57) Li, K.-M.; Jiang, J.-G.; Tian, S.-C.; Chen, X.-J.; Yan, F. Influence of Silica Types on Synthesis and Performance of Amine−Silica Hybrid Materials Used for CO_2 Capture. *J. Phys. Chem. C* **2014**, *118* (5), 2454−2462.
(58) Zhao, J.; Simeon, F.; Wang, Y.; Luo, G.; Hatton, T. A. Polyethylenimine-impregnated Siliceous Mesocellular Foam Particles

as High Capacity CO_2 Adsorbents. *RSC Adv.* **2012**, *2* (16), 6509−6519.
(59) Liu, Q.; Shi, J.; Zheng, S.; Tao, M.; He, Y.; Shi, Y. Kinetics Studies of CO_2 Adsorption/Desorption on Amine-Functionalized Multiwalled Carbon Nanotubes. *Ind. Eng. Chem. Res.* **2014**, DOI: 10.1021/ie502009n.
(60) Tumuluri, U.; Isenberg, M.; Tan, C.-S.; Chuang, S. S. C. In Situ Infrared Study of the Effect of Amine Density on the Nature of Adsorbed CO_2 on Amine-Functionalized Solid Sorbents. *Langmuir* **2014**, DOI: 10.1021/la501284y.
(61) Yamdagni, R.; Kebarle, P. Gas-phase Basicities of Amines. Hydrogen Bonding in Proton-bound Amine Dimers and Proton-induced Cyclization of.Alpha., .Omega.-diamines. *J. Am. Chem. Soc.* **1973**, *95* (11), 3504−3510.
(62) Knöfel, C.; Martin, C. l.; Hornebecq, V.; Llewellyn, P. L. Study of Carbon Dioxide Adsorption on Mesoporous Aminopropylsilane-Functionalized Silica and Titania Combining Microcalorimetry and in Situ Infrared Spectroscopy. *J. Phys. Chem. C* **2009**, *113* (52), 21726−21734.

NOTE ADDED AFTER ASAP PUBLICATION

This paper was published on the Web on August 4, 2014, with the incorrect artwork for Figures 1 and 2. The corrected version was reposted on August 6, 2014.